Monochromatic single photon events at the muon collider

M. Casarsa,[1] M. Fabbrichesi,[1] and E. Gabrielli[2,1,3]
[1]*INFN, Sezione di Trieste, Via Valerio 2, 34127 Trieste, Italy*
[2]*Physics Department, University of Trieste, Strada Costiera 11, 34151 Trieste, Italy*
[3]*Laboratory of High-Energy and Computational Physics, NICPB, Ravala 10, 10143 Tallinn, Estonia*

(Received 6 December 2021; accepted 17 March 2022; published 11 April 2022)

The cross section for lepton pair annihilation into a photon and a dark photon or an axionlike particle is constant for large center-of-mass energies because some of the portal operators coupling the Standard Model and dark sector are proportional to the energy. Feebly coupled though they are, these portal operators will be enhanced by the large center-of-mass energy made available by a muon collider and thus provide the ideal example of possible physics beyond the Standard Model to be studied with such a machine. We discuss the characteristic signature of the presence of these operators: monochromatic single photon events for the two benchmarks of having center-of-mass energies of 3 and 10 TeV and integrated luminosity of, respectively, 1 and 10 ab^{-1}. We find that an effective scale of the portal operator as large as $\Lambda = 112$ TeV for an axionlike particle and $\Lambda = 141$ TeV for a dark photon can be separated from the background with a confidence level of 95% in the first benchmark; these interaction scales can be raised to $\Lambda = 375$ and 459 TeV in the case of the second benchmark. The signal for the pseudoscalar particle can be distinguished from that of the spin-1 with about 500 events. The response of the detector to high-energy photons is examined.

DOI: 10.1103/PhysRevD.105.075008

I. INTRODUCTION

Interest in designing and building a muon collider [1,2] will be directly proportional to the capability of such a collider of exploring not only the Standard Model with great precision but also physics beyond it [3,4]. Many a dedicated study has already been performed, mostly for the physics of the Higgs boson [5] but also on precision electroweak physics [6,7], vector boson fusion processes [8], lepto-quarks discovery [9], and possible dark matter candidates [10]. It is in this spirit that we consider the possibility of probing the physics of a dark sector at a muon collider.

Dark sectors are made of states that are singlets under the Standard Model gauge groups [11]. If they had no other interaction with ordinary matter, they would be invisible but for large-scale gravitational effects, the same way as dark matter is. To make these states accessible to our probes, they are also assumed to have some interaction, dubbed the *portal*, to Standard Model particles; this interaction is sufficiently feeble to allow for light states, and, indeed, even massless states of the dark sector to be as yet undetected. The search for these elusive dark particles has been carried on so far in various dedicated experiments (see Ref. [11] for a recent review).

Dark particles can couple to Standard Model states by means of effective higher dimensional operators—starting from and, for all practical purposes, dominated by dimension 5 operators. These operators appear for instance in dark-photon coupling to Standard Model fermions via magnetic dipole interactions [12,13], as predicted by portal dark-sector models [14,15], or axionlike particles to diphoton couplings, as a consequence of the $U(1)$ Peccei-Quinn anomaly [16–18]. On dimensional grounds, the production cross section of a dark particle in association with a photon at high energy tends to a constant proportional to $1/\Lambda^2$, with Λ the effective scale associated to the dimension five operators. This behavior must be compared to that of the cross section for dark particles production by renormalizable couplings to Standard Model particles, the cross section of which is expected to decrease as $\sigma \sim 1/s$ at a high center of mass (c.m.) energy $\sqrt{s}$. On the other hand, the corresponding cross section for the Standard Model background, characterized by a photon plus a neutrino pair, scales as $1/s$ at high energy [19,20], which leads to the enhanced ratio of signal over background at high energy for dark-particle productions in association to a photon.

This feature makes a collider with both high energy and high luminosity a very promising machine for the study of the dark sector. The muon collider is a case in point. Such a

collider can provide the simplest, but also the most striking, signature of the existence of a dark sector: the annihilation of the muon pair into a light dark particle and a single photon. As the dark particle is invisible and assumed to be light, the event is a monochromatic single photon with almost half of the c.m. energy.

We study the aforementioned signature for the two benchmark scenarios of a muon collider with c.m. energy of 3 and 10 TeV. The integrated (5 years) luminosity is taken to be of, respectively, 1 and 10 ab^{-1}. The signal is enhanced over the background by the large energy though several background events persist in the same energy region because of the radiative return of the Z-boson pole and a statistical analysis is necessary in order to distinguish the signal from this background. The monochromatic signature at muon collider induced by the radiative return effect for heavy Higgs bosons has been analyzed in [21].

Our analysis shows that, within the first five years of operation, the muon collider will be able to set new and more stringent limits to the effective couplings of dark photon and axionlike particles to muons and photons. The nature of the dark sector particle, whether is a pseudoscalar coupled to photons or a spin-1 coupled to muons, can also be decided within the first five years of operation. We also discuss in detail the response of the detector to high-energy photons.

Previous work on the dark sector along similar lines includes [22], where the axionlike particle (ALP) coupling to photons is studied at hadron colliders [23,24], where limits on the same coupling are estimated for the CLIC and FCC-ee colliders, and [25], where the ALP couplings are studied at fixed-target experiments (for instance for the PADME experiment). Our work is the first to discuss the separation from the background of the monophoton signal and the implementation to the muon collider. Experimental searches for the same monophoton signature have been performed at the LEP [26–28], the Tevatron [29,30], and the LHC [31,32] though only providing rather weak bounds.

A. Dark photons and axionlike particles

Here we consider two possible candidates for the invisible state in the single photon signature: a massless, spin 1 particle (the dark photon [12,13]) and a light pseudoscalar particle [17,18,33] (axionlike in its properties).

The dark photon (DP) A'_μ with field strength $F'^{\mu\nu}$ can couple to the muons via the magnetic-dipole interaction with Pauli dipole term

$$\mathcal{L}_{\text{DP}}^{\text{dipole}} = \frac{1}{2\Lambda}(\bar{\mu}\sigma_{\mu\nu}\mu)F'^{\mu\nu}, \tag{1}$$

where $\sigma_{\mu\nu}$ is defined to be $i[\gamma^\mu,\gamma^\nu]/2$. The scale Λ modulates the strength of the interaction. In a UV completion of the theory the effective scale Λ can be generated at one loop by the exchange of heavy particles in the portal sector [14,15]. The operator in Eq. (1) originates from a $SU(2)_L$ invariant dimension-six operator of the form $(\bar{L}\sigma_{\mu\nu}\mu_R)HF'^{\mu\nu} + \text{H.c.}$, where H and L are the $SU(2)_L$ Higgs and muon-lepton doublets, respectively. Here we consider only its contribution in the broken electroweak phase, by replacing the Higgs fields with its vacuum expectation value, as expressed in Eq. (1).

The coupling in Eq. (1) is the only one in the case of a massless dark photon. In the massive case,[1] the Pauli operator in Eq. (1) has not been constrained by current massive DP searches because all of them have been performed at low energies ($\sqrt{s} \ll \Lambda$) where its contribution is suppressed by terms of order s/Λ^2. It however becomes relevant at the higher energies of a muon collider. The effective interaction approach is consistent as long as the effective scale Λ is assumed to be larger or at most of the same order as the c.m. energy.

The ALP a couples to the muons by means of the portal operator

$$\mathcal{L}_{\text{ALP}}^{\text{muon}} = \frac{1}{\Lambda}(\bar{\mu}\gamma_5\gamma^\mu\mu)\partial_\mu a \tag{3}$$

and to photons by means of

$$\mathcal{L}_{\text{ALP}}^{\text{photon}} = \frac{1}{\Lambda}aF^{\alpha\beta}\tilde{F}_{\alpha\beta}, \tag{4}$$

where $\tilde{F}_{\alpha\beta} = 1/2\epsilon_{\alpha\beta\mu\nu}F^{\mu\nu}$ is the dual field strength of the photon, with $\epsilon_{\alpha\beta\mu\nu}$ the Levi-Civita antisymmetric tensor satisfying $\epsilon_{0123} = 1$. For on shell ALP production the interaction in Eq. (3) is equivalent to the renormalizable interaction $(m_\mu/\Lambda)(\bar{\mu}\gamma_5\mu)a$, whose coupling is proportional to the muon mass m_μ over the Λ scale and therefore chirally suppressed. We restrict our analysis to the ALP production via the effective interaction in Eq. (4). The effective field theory expansion is in this case consistent as long as $\sqrt{s} < \Lambda$.

To make contact with the notation of the experiment searches for these interactions, we notice that the coupling in the dipole operator in Eq. (1) is usually expressed in the literature as the (dimensionful) coefficient $g_{a\mu} = 2/\Lambda$ for the experiments probing the interaction between ALP and muons, which can be identified with ours for the DP because of the similar structure of the effective operators in

[1]In addition to the Pauli dipole term, the massive dark photon has also an ordinary coupling to the vectorial muon current

$$\mathcal{L}_{\text{DP}}^{\text{tree}} = \varepsilon e(\bar{\mu}\gamma^\mu\mu)A'_\mu, \tag{2}$$

arising from a tree-level contribution of kinetic mixing of dark photons with an ordinary photon [12] that in the massive case cannot be rotated away.

Eqs. (1) and (3). In a similar manner, the ALP-photons interaction in Eq. (4) is usually expressed in the literature by means of the coefficient $g_{a\gamma} = 4/\Lambda$.

B. Constraints

The possibility of seeing DP or ALP at a collider experiment depends on the size of the effective scale Λ controlling their interaction with ordinary matter and photons. For the interaction between muons and DP, this scale is mostly constrained by the value of the anomalous magnetic moment $(g-2)$, the number of relativistic species in the early Universe [Cosmic Microwave Background (CMB)] and the energy emission of Supernova 1987A (SN). Figure 1 summarizes these three constraints for the DP in terms of the effective coupling $1/\Lambda$ and gives the relative references.

The very strong SN bound makes impossible even for a muon collider to explore this interaction. For this reason, we mostly assume that the dark sector particles are massive with a mass of at least 10 MeV, an energy scale that makes their production in cosmological and astrophysical process suppressed.

The coupling between ALP and photons is constrained by direct searches and from SN1987A data. In this case, however, the limit stops for stronger couplings leaving values $10^2 < \Lambda/\mathrm{GeV} < 10^5$ possible (again, for a mass larger than 10 MeV). Figure 2 summarizes the current limits in terms of $g_{a\gamma} = 4/\Lambda$ and shows future bounds, those in this article included.

We assume that DP and ALP decays are dominated by those into dark sector particles so that their signature remains as missing energy. For this reason, bounds like those from beam dump and other experiments, coming from the decay into visible states are not included. We comment below on what range of masses and coupling are consistent with a non-negligible branching rate into Standard Model states.

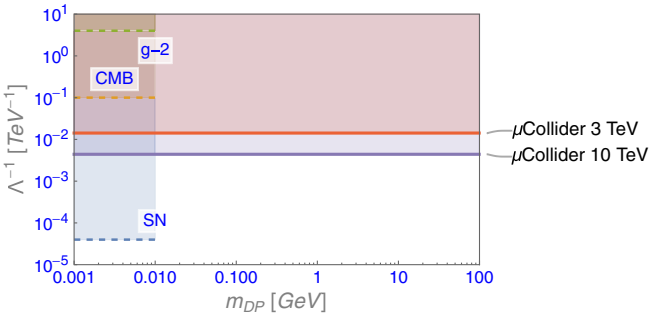

FIG. 1. Limits on DP effective coupling Λ to muons as defined in Eq. (1), as a function of the dark-photon mass $m_{A'}$: for SN the scale of the coupling to muons has been set at $10^{4.4}$ TeV [34] by the effect of dark radiation on supernovae dynamics. For CMB see Ref. [35]. For $g-2$ see Refs. [36,37]. For masses up to 100 GeV the μCollider limits are for all practical purposes mass independent.

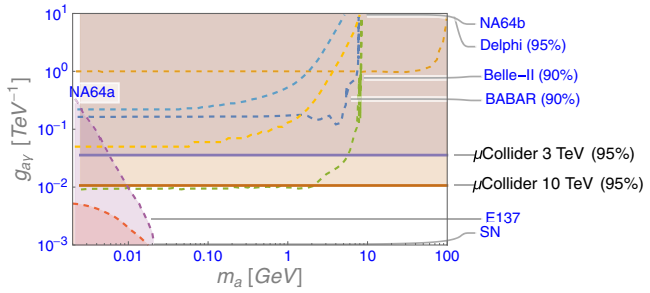

FIG. 2. Limits on $g_{a\gamma} = 4/\Lambda$ as a function of the ALP mass m_a: NA64a [38], Delphi [39], and *BABAR* [40] are actual limits. Belle-II [41,42], NA64b [38], and μCollider [this paper] are future estimates. The limit indicated by E137 is the one from [43] as modified for a small (10^{-4}) visible branching fraction [25]. For masses up to 100 GeV the μCollider limits are for all practical purposes mass independent.

The relevant Feynman diagrams are shown in Fig. 3. These two are the only diagrams contributing in the high-energy regime because the direct coupling of the ALP to muons is not enhanced by going to large c.m. energies.

C. The background: $\mu^+\mu^- \to \gamma\nu\bar{\nu}$

The Standard Model process $\mu^+\mu^- \to \gamma\nu\bar{\nu}$ gives rise to the same signature as the signal we are after. The analytical expression for the double differential cross section in the solid angle and photon energy is provided in [19] and in the low energy regime in [20]. Figure 4 shows the E_γ and $\cos(\theta_\gamma)$ distributions for the background events. The cross section grows with the c.m. energy but the number of events with a high-energy photon decreases. Events at the end of the photon energy spectrum around

$$E_\gamma = \frac{\sqrt{s}}{2}\left(1 - \frac{m_Z^2}{s}\right) \tag{5}$$

are enhanced by the radiative return of the Z-boson pole. This feature (unfortunate, for our analysis) reduces the sensitivity to the signal that—it being a two-body

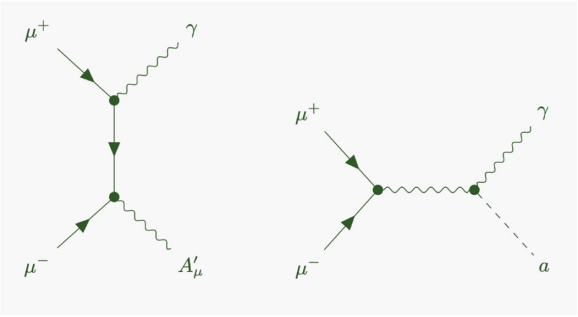

FIG. 3. The diagrams contributing to the processes $\mu^+\mu^- \to \gamma A'_\mu$ (left) and $\mu^+\mu^- \to \gamma a$ (right) in the high-energy regime. For masses up to 100 GeV the μCollider limits are mass independent.

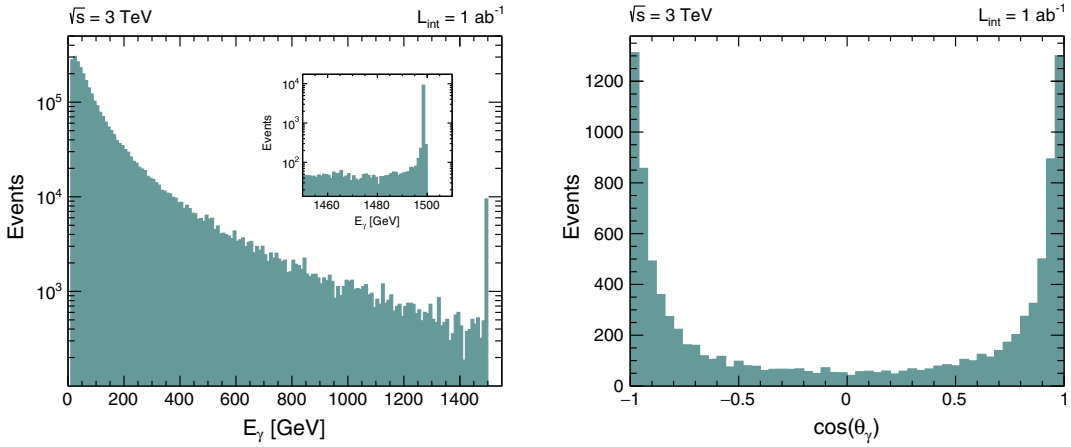

FIG. 4. Background process $\mu^+\mu^- \to \gamma\nu\bar{\nu}$: the distributions in E_γ and $\cos(\theta_\gamma)$ (the latter for energies larger than 1490 GeV) of the monophotons. The inset in the left panel shows the tail of the energy distribution. Notice the peak at the end of the energy spectrum due to the radiative return of the Z-boson pole.

process—is centered in the same range of energies (for $s \gg m_Z^2$).

D. Decay length

If the decay into Standard Model states is non-negligible (or the dominant one), then the decay length

$$L = |\vec{\beta}|\tau = \frac{\sqrt{s}}{2m\Gamma}\left(1 - \frac{m^2}{s}\right) \tag{6}$$

for a dark state of mass m and width Γ, with $\sqrt{s}$ the muon c.m. energy, may turn out to be inside the detector turning the invisible into a visible track.

Assuming the minimal requirement of a massive dark photon coupled via magnetic-dipole type of operator to muons, decaying into two muons and assuming axion decaying mainly into two photons, we have for the corresponding decay widths the following results:

$$\Gamma(A' \to \mu^+\mu^-) = \frac{m_{A'}^3(1-4r)^{1/2}(1+8r)}{24\pi\Lambda^2},$$
$$\Gamma(a \to \gamma\gamma) = \frac{m_a^3}{4\pi\Lambda^2}, \tag{7}$$

where $r = m_\mu^2/m_{A'}^2$, with m_μ, m'_A, and m_a as the masses of the muon, dark photon, and axion, respectively. The assumption of a single decay channel provides an upper bound on the decay length consideration. In particular, the requirement that the state decay outside the decay length L gives the following lower bound of Λ versus the corresponding boson mass $m_{A'}$ or m_a,

$$\Lambda > m_{A'}^2 \frac{L^{1/2}}{s^{1/4}} \frac{(1-4r)^{1/4}(1+8r)^{1/2}}{2\sqrt{3\pi}(1-m_{A'}^2/s)^{1/2}} \quad \text{for DPs},$$
$$\Lambda > m_a^2 \frac{L^{1/2}}{s^{1/4}} \frac{1}{\sqrt{2\pi}(1-m_a^2/s)^{1/2}} \quad \text{for ALPs}. \tag{8}$$

We show in Figs. 5 and 6 the contour plots of the decay length as a function of the DP and ALP masses and the

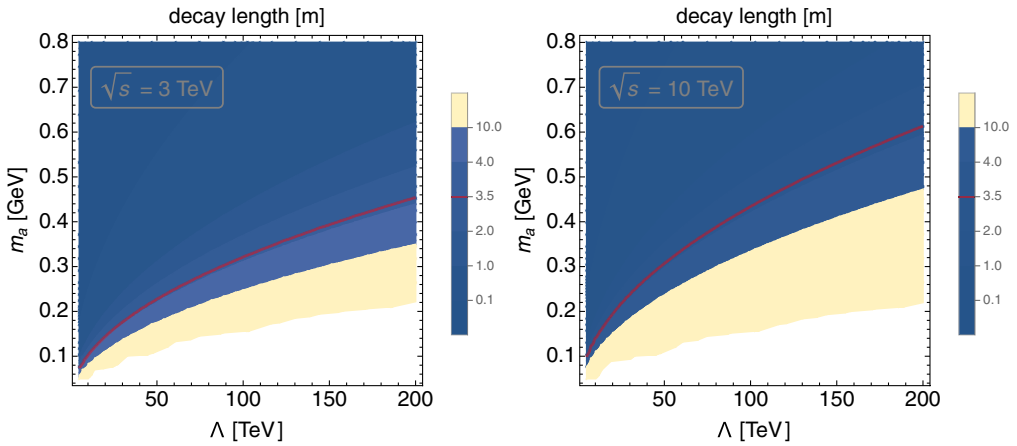

FIG. 5. Decay length (in meters) for the ALP as a function of its mass m_a and the interaction scale Λ. The contour in red marks the size of the detector (3.5 meter).

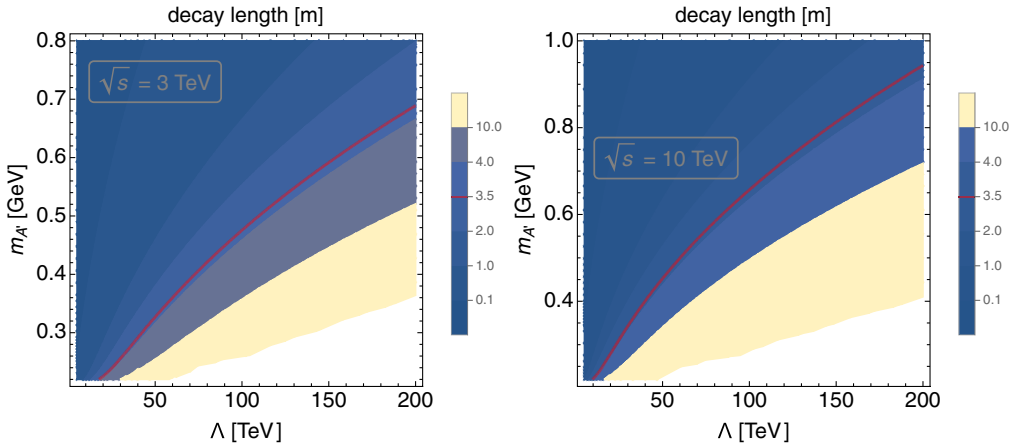

FIG. 6. Same as in Fig. 5 for the DP.

corresponding scale Λ, assuming only the interactions in Eqs. (1) and (4) for the dark photon and axion, respectively. For masses below approximately 300 MeV (3 TeV) and 400 MeV (10 TeV), and for energy scales in the coupling as those we explore (which are around and above 100 TeV), the decay length lays outside the detector (taken here to be about 3.5 meter wide) for the ALP. The same occurs for masses below approximately 500 MeV (3 TeV) and 600 MeV (10 TeV) for the DP. For masses above these ranges the decay may occur inside the detector. For such values we assume the DP and ALP to decay mostly into dark states and remain invisible.

II. METHODS

A. Muon collider

Among the projects currently under study for the generation of particle accelerators following the LHC, the muon collider represents a unique machine that has the capability to provide leptonic collisions in a multi-TeV energy range [1]. Such a great physics potential is accompanied by unprecedented technological challenges on the experimental side due to the fact that muons are unstable particles. The electrons and positrons, created in muon decays, and the photons radiated by them interact with the machine elements and produce an intense flux of $O(10^{10})$ secondary and tertiary particles (photons, neutrons, electrons and positrons, charged hadrons, muons) that eventually may reach the detector. The amount and the characteristics of the beam-induced background in the detector depend on the collider energy and the machine optics and lattice elements. The main features of beam-induced background particles are relatively soft momenta (a few MeV for the electromagnetic component, half a GeV for the hadronic component, and a few tens GeV for muons) and asynchronous arrival times to the detector with respect to the collisions [44].

The exploitation of the full physical potential that a muon collider can offer will depend on the capacity of the experiment to mitigate and cope with the beam-induced background through cutting-edge technologies and a dedicated design of the machine-detector interface and the detector (optimized geometry, high granularity, timing information), new sophisticated algorithms for pattern recognition and reconstruction of physical objects [45,46]. In this study, we assume that this is the case and the physical objects we are using are not significantly affected by the beam-induced background.

The International Muon Collider Collaboration [1] is currently focusing on two muon collider conceptual designs: a 3 TeV collider providing an instantaneous luminosity of a few 10^{34} cm^{-2} s^{-1} and a machine at $\sqrt{s} = 10$ TeV or above with an instantaneous luminosity of a few 10^{35} cm^{-2} s^{-1}. Accordingly, in our analysis, we consider two benchmark scenarios:

S1: c.m. energy of 3 TeV and total integrated luminosity of 1 ab^{-1},

S2: c.m. energy of 10 TeV and total integrated luminosity of 10 ab^{-1},

and study the generation of events with a single, monochromatic photon plus missing energy in the final states.

B. Event generation and detector simulation

The events for the signal and the background are generated by means of MADGRAPH5 [47]. A 10 GeV cut on the photon generated transverse momentum is imposed to remove most of the soft radiation. The output of MADGRAPH5 is automatically fed into PYTHIA [48,49] and the events thus generated are processed by the detector simulation.

The simulation of the detector is one of the crucial steps in making the study of physics at the muon collider possible. An agreed upon standard is yet to be defined. We utilize detector full simulation tools based on CLIC's ILCSoft framework [50]. The detector model is based on CLIC's detector concept [51], which comprises a full-silicon tracking system, hermetic high-granularity electromagnetic

and hadronic calorimeters, and a muon spectrometer. The tracking detectors and the calorimeters are immersed in a 3.57 Tesla solenoidal magnetic field. The vertex detector and the machine-detector interface have been adapted to cope with the harsher background environment at a muon collider: the geometry of the vertex detector is optimized to minimize the occupancy from beam-induced particles and two tungsten conical shields, placed around the beam pipe inside the detector, reduce the background levels in the detector by approximately three orders of magnitude.

The sub-detectors used in this analysis are the electromagnetic (ECAL) and the hadronic (HCAL) calorimeters. The ECAL and HCAL are both sampling calorimeters. The ECAL consists of 40 layers of 1.9-mm tungsten absorber and 5×5 mm^2 silicon pad sensors for a total of 22 radiation lengths, whereas the HCAL has 60 layers of 19-mm steel absorber and 30×30 mm^2 plastic scintillating tiles, which correspond to 7.5 nuclear interaction lengths.

C. Event reconstruction and selection

The full-simulated events are reconstructed with a particle-flow algorithm [52], which is integrated in the ILCSoft reconstruction software. The photon signature in the detector is represented by an isolated electromagnetic shower in the ECAL, to which no charged particle trajectory is associated. The photon four-momentum is determined from the energy measured in the ECAL and the photon line of flight, taken as the direction from the primary interaction vertex to the position of the energy deposit.

A sample with a single photon per event was used to determine and tune the detector performance in reconstructing and identifying high-energy photons. The photons, generated in the nominal collision vertex at the center of the detector, are uniformly distributed in energy between 1 GeV and 5 TeV, in polar angle between 10° and 170°, and in the full azimuthal angle range. The photon sample was processed with the detector full simulation and reconstructed with the same algorithms as those used for the signal and background samples.

It results that a few percent of the energy released by high-energy photons in the ECAL spills into the HCAL. Therefore, for a more accurate reconstruction of such photons, the HCAL energy is recovered and added to the energy of the closest spatially compatible ECAL deposit. In the same sample, the photon reconstruction performance is assessed: photons with $E_\gamma \gtrsim 10$ GeV are reconstructed with an efficiency close to 100%, while the photon relative energy resolution is lower than 0.7% for $E_\gamma \gtrsim 1500$ GeV. Moreover, corrections are calculated and applied to the photon reconstructed energy to make the detector response uniform as a function of photon energy and polar angle.

Events are selected for the analysis if only one photon has been reconstructed inside the detector angular acceptance $10° < \theta_\gamma < 170°$. The signal is strengthened against the background by two simple kinematical cuts:

(i) Photon energy: $E_\gamma > 1450$ GeV for $\sqrt{s} = 3$ TeV and $E_\gamma > 4800$ GeV for $\sqrt{s} = 10$ TeV.
(ii) Photon polar angle: $40.4° < \theta_\gamma < 139.6°$.

These optimize the selection process of the events around the end of energy spectrum where the signal is. In the 3-TeV analysis, this selection yields 3020 background events. The DP signal events range between 193 and 104 as Λ increases from 110 to 150 TeV, whereas the ALP signal events range between 184 and 59 as Λ increases from 85 to 130 TeV. In the 10-TeV analysis, this selection yields 2630 background events. The DP signal events range between 160 and 96 as Λ increases from 380 to 490 TeV; the ALP signal events range between 174 and 77 as Λ increases from 280 to 420 TeV.

Beside the physical backgrounds from SM processes, we have investigated an additional potential source of experimental backgrounds that might mimic the monophoton signature we are looking for. Using a sample of $\mu^+\mu^- \to \gamma\gamma$ events at $\sqrt{s} = 3$ TeV, we studied the case of two-photon events, in which one of the photons is not reconstructed, and found such a background negligible.

For completeness, we also considered a potential background from events with an energetic electron misidentified as a photon. The electron misidentification rate was estimated in a sample of single electrons, processed through the detector full simulation and reconstruction. It is found to be lower than 1% in the central region of the detector, making also this background negligible.

III. RESULTS

To assess the reach of the muon collider to the considered dark-sector signals, we test the signal strength for different values of Λ against the background-only hypothesis. The observable that is found to better discriminate the signal from background events is the photon transverse momentum: the distributions in p_T^γ of the signal and the background differ significantly, with the Standard Model background presenting a long tail toward smaller momenta. These two distributions are used to define a likelihood for the background-only ($\mathcal{L}_\mathrm{B}$) and the background plus signal hypotheses ($\mathcal{L}_\mathrm{S+B}$).

The probability distribution functions (pdf) for the null hypothesis (background only) and the alternative hypothesis (background plus signal) can be extracted directly from the dependence on p_T^γ. The signal pdf ($\mathrm{pdf_S}$) is parametrized with a crystal-ball function centered at $\sqrt{s}/2$, while the background pdf ($\mathrm{pdf_B}$) is modeled with a complementary error function plus a Gaussian.

We take $N_\mathrm{obs}^{(S)}$ signal events as well as $N_\mathrm{obs}^{(\mathrm{B})}$ background events generated according to the corresponding pdfs. Each event i is characterized by the value of p_T^γ. The likelihood function, for example for the signal plus background hypothesis, is given by

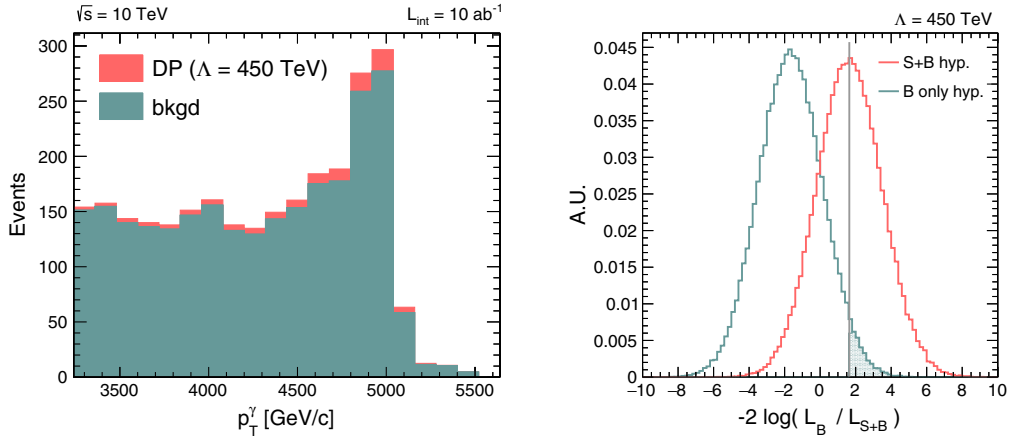

FIG. 7. Distribution of the photon transverse momenta at $\sqrt{s} = 10$ TeV (left). A dark photon signal, corresponding to $\Lambda = 450$ TeV, is stacked on top of the background distribution. The p_T^γs reconstructed above 5000 GeV are due to detector resolution effects and a remnant of the energy correction procedure. In the right panel, the LLR distributions for the background-only and background-plus-signal hypotheses are shown.

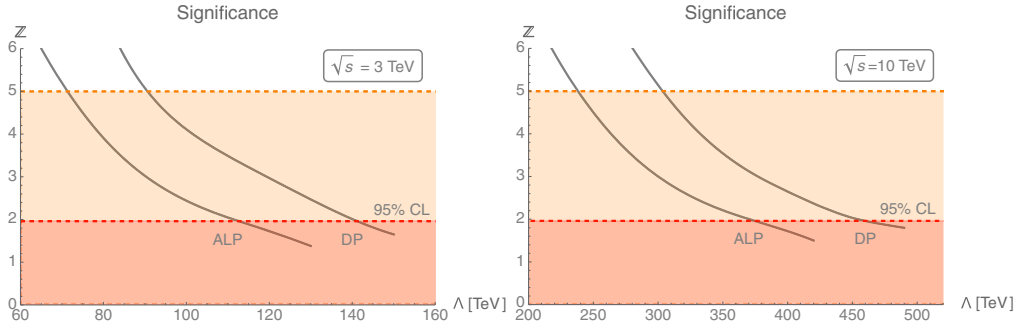

FIG. 8. Significance for DP and ALP at $\sqrt{s} = 3$ TeV (left) and at $\sqrt{s} = 10$ TeV (right) as a function of the interaction scale Λ. Red dashed line corresponds to 95% CL, orange dashed line to 5σ (discovery reach). The curves are obtained by running the simulation with a mass of 1 GeV for the DP or the ALP. The cross section is independent of the mass of the DP or ALP, in the regime of several TeV we are exploring, as long as they are below 100 GeV.

$$\mathcal{L}_{\mathrm{S+B}} = e^{-N_{\mathrm{obs}}^{(S)} - N_{\mathrm{obs}}^{(\mathrm{B})}} \times \prod_i^{N_{\mathrm{obs}}} [N_{\mathrm{obs}}^{(S)} \times \mathrm{pdf}_{\mathrm{S}}(p_i^T) + N_{\mathrm{obs}}^{(\mathrm{B})} \times \mathrm{pdf}_{\mathrm{B}}(p_i^T)], \tag{9}$$

where the events p_i^T are taken from the S and B populations. In this way, it is possible to randomly generate N_{obs} events and compute the logarithm of the likelihood ratio (LLR) defined by

$$\mathrm{LLR} = -2 \log \frac{\mathcal{L}_{\mathrm{B}}}{\mathcal{L}_{\mathrm{S+B}}}. \tag{10}$$

By repeating this pseudoexperiment N_{ps} times, we construct a sample that can be used to compute the LLR statistical distribution for the two hypotheses. We take $N_{\mathrm{ps}} = 10^5$.

We construct two statistical samples for the LLR, the first one with events characterized by the value of p_i^T generated according to the background-only population, the second one with p_i^T generated according to the signal plus background population. Figure 7 shows the p_T^γ distribution for signal and background events and the result for the LLR analysis in the case of the dark photon at $\sqrt{s} = 10$ TeV.

To quantify the difference in terms of statistical significance, we compute the p value of the median of the signal-plus-background LLR distribution by integrating the background-only curve from the median value (indicated

TABLE I. Explorable values of the effective energy scale Λ for DP and ALP (95% CL) for the two benchmark scenarios of the future muon collider under consideration.

	$\sqrt{s} = 3$ TeV		$\sqrt{s} = 10$ TeV	
	DP (TeV)	ALP (TeV)	DP (TeV)	ALP (TeV)
Limit	141	112	459	375
Discovery	92	71	303	238

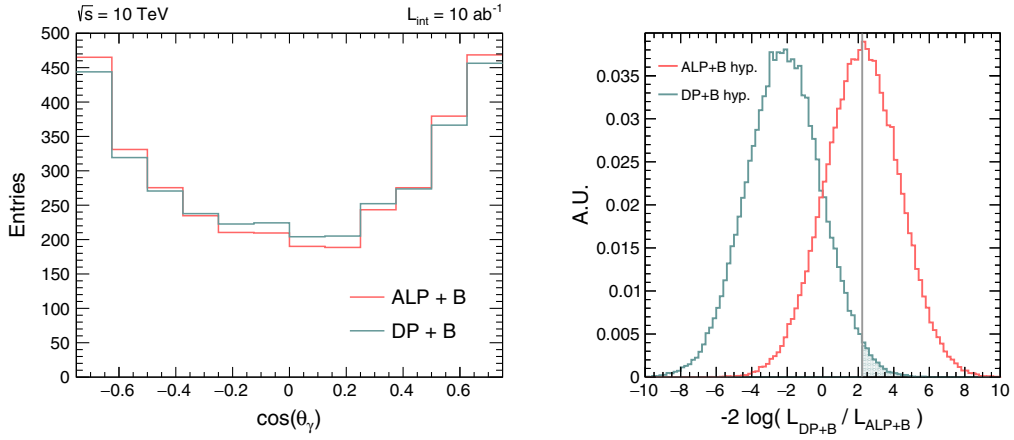

FIG. 9. On the left: total angular distributions of the ALP and DP signals plus the background (B). 500 events are assumed for both signals. On the right: LLR of the corresponding hypotheses.

by the gray vertical line in Fig. 7) to $+\infty$. The significance is defined as $\mathcal{Z} = \Phi^{-1}(1-p)$ where

$$\Phi(x) = \frac{1}{2}\left[1 + \mathrm{erf}\left(\frac{x}{\sqrt{2}}\right)\right]. \tag{11}$$

The value of $\mathcal{Z}$ assigns a statistical significance to the separation between the two LLR distributions. We can take $\mathcal{Z}$ as the number of σs, in the approximation in which the distribution is assumed to be Gaussian, and translates the number of σs into a confidence level (CL).

The significance thus obtained scales as $1/\Lambda^2$. We can plot the significance as a function of Λ and find the effective scale value at which it is equal to 1.96. The value thus found corresponds to the largest value of Λ for which we can separate the signal from the background with a CL of 95%.

Figure 8 shows the determination of the scale Λ for which the separation of the signal from the background reaches the 95% CL for both the DP and the ALP at the two c.m. energies under consideration. Table I gives the values of Λ for the DP and ALP thus determined. The same table also gives the discovery (5σ) for the largest Λ reachable.

These results can be compared with current and future limits from cosmological, astrophysical and collider physics we discussed in the Introduction. In Fig. 2 all the available limits for the coupling between the DP and muons are plotted together. A backward glance shows that

(i) For massless DP the coupling is constrained by the SN events to a very small value, much smaller than those explorable at the muon collider;
(ii) For massive DP and masses above 10 MeV the muon collider could provide new (and very stringent) limits.

The same is done for the limits for the coupling between the ALP and the photon in Fig. 1. We see in this case that the muon collider could provide the best limits even though the estimated reach of Belle-II seems to overlap with that of the muon collider at c.m. energy of 10 TeV.

A. Distinguishing the DP from the ALP

Assuming that a signal has been seen, will it be possible to determine whether it comes from a DP or an ALP? The difference rests on their characteristic angular distributions: while the DP angular distribution is flat, the ALP shows an angular dependence.

By means of a statistical analysis similar to that of the previous section, we defined two likelihood functions, $\mathcal{L}_{\mathrm{DP+B}}$ and $\mathcal{L}_{\mathrm{ALP+B}}$, including angular pdfs for the signal and the background components in Eq. (9). The signal pdfs are parametrized as functions of $\cos(\theta_\gamma)$ with a constant and a second order polynomial for the DP and the ALP hypotheses, respectively. The background pdf is a second order polynomial. Figure 9 shows a comparison of the total angular distributions for the two cases and the corresponding LLR distributions.

We find that 500 events are necessary to distinguish with 95% CL between the spin-0 (ALP) and the spin-1 (DP) hypotheses. For a scale $\Lambda \simeq 160$ TeV, this number of events is accumulated approximately in five years. A comparable number of events is necessary at $\sqrt{s} = 3$ TeV.

IV. CONCLUSIONS

The exploration of the physics program at a future muon collider has just begun. In this paper, we study the potential of the monophoton signature in the search for a dark sector. The high energy and luminosity made available by the muon collider make it the ideal machine to study those interactions between the Standard Model and the dark sector from dimension-five portal operators that grow with the energy, namely, those of the DP and the ALP. Although the sensitivity of the analysis is hampered by the radiative return of Z-boson pole—which makes the cross section of the background non-negligible at the end of the energy

spectrum of the photons—we find that a muon collider could provide a competitive determination of the effective scale of the relevant operators.

A suitable choice of cuts on the photon energy and polar angle, to suppress the large background induced by the radiative return effect, has been implemented to increase signal over background sensitivity. We considered two benchmark scenarios corresponding to collision center-of-mass energies of 3 and 10 TeV, and integrated (5 years) luminosities of 1 and 10 ab^{-1}, respectively. In the case of nonobservation of a signal, lower bounds at 95% CL on the interaction scale Λ for the dark-photon and ALP couplings have been derived for the 3 TeV collider corresponding to $\Lambda = 141$ and $\Lambda = 112$ TeV, respectively, that can be raised to $\Lambda = 375$ and 459 TeV for the 10 TeV energy collisions, respectively. A more sophisticated physical analysis based on two-dimensional cuts or multivariate techniques, which we leave to future work, may further improve the above sensitivities to the effective scale Λ.

When and if a signal is found, it will be important to know which dark sector particle is responsible for it. We show that a muon collider operating at 3 or 10 TeV has the potential to distinguish the spin-0 ALP from the spin-1 DP scenario. For a common energy scale $\Lambda = 300$ TeV—about 500 events (which can be approximatively accumulated in five years) are required to separate the two spin scenarios at the 95% CL.

Our analysis shows that a muon collider can provide a powerful tool in searching for dark particles because of its high sensitivity to the interactions scales of dark-boson portals, the clean environment of lepton collisions and the high luminosity.

ACKNOWLEDGMENTS

This work was performed within the Muon Collider Detector Design and Performance group [53]. The digital inclusion of some of the experimental limits in the figures was done by means of WEBPLOTDIGITIZER [54]. M. C. thanks Federico Meloni for his comments and feedback. M. F. is affiliated to the Physics Department of the University of Trieste and SISSA—the support of which is acknowledged. M. F. and E. G. are affiliated to the Institute for Fundamental Physics of the Universe, Trieste, Italy.

[1] K. Long, D. Lucchesi, M. Palmer, N. Pastrone, D. Schulte, and V. Shiltsev, Muon colliders to expand frontiers of particle physics, Nat. Phys. **17**, 289 (2021).

[2] J. P. Delahaye, M. Diemoz, K. Long, B. Mansoulié, N. Pastrone, L. Rivkin, D. Schulte, A. Skrinsky, and A. Wulzer, Muon colliders, arXiv:1901.06150.

[3] M. Greco, Physics potential and motivations for a muon collider, Int. J. Mod. Phys. A **31**, 1630028 (2016).

[4] H. Al Ali, N. Arkani-Hamed, I. Banta, S. Benevedes, D. Buttazzo, T. Cai, J. Cheng, T. Cohen, N. Craig, M. Ekhterachian *et al.*, The Muon Smasher's guide, arXiv:2103.14043.

[5] V. D. Barger, M. S. Berger, J. F. Gunion, and T. Han, Higgs boson physics in the s channel at $\mu^+\mu^-$ colliders, Phys. Rep. **286**, 1 (1997); T. Han and Z. Liu, Potential precision of a direct measurement of the Higgs boson total width at a muon collider, Phys. Rev. D **87**, 033007 (2013); A. Conway and H. Wenzel, Higgs measurements at a muon collider, arXiv:1304.5270; Y. Alexahin, C. M. Ankenbrandt, D. B. Cline, A. Conway, M. A. Cummings, V. Di Benedetto, E. Eichten, C. Gatto, B. Grinstein, J. Gunion *et al.*, Muon collider Higgs factory for snowmass 2013, arXiv:1308.2143; G. J. Gounaris and F. M. Renard, Test of the triple Higgs boson form factor in $\mu^-\mu^+ \to HH$, Phys. Rev. D **93**, 093018 (2016); T. Han, D. Liu, I. Low, and X. Wang, Electroweak couplings of the Higgs boson at a multi-TeV muon collider, Phys. Rev. D **103**, 013002 (2021); M. Chiesa, F. Maltoni, L. Mantani, B. Mele, F. Piccinini, and X. Zhao, Measuring the quartic Higgs self-coupling at a multi-TeV muon collider, J. High Energy Phys. 09 (2020) 098.

[6] D. Buttazzo, R. Franceschini, and A. Wulzer, Two paths towards precision at a very high energy lepton collider, J. High Energy Phys. 05 (**2021**) 219.

[7] T. Han, D. Liu, I. Low, and X. Wang, Electroweak couplings of the Higgs boson at a multi-TeV muon collider, Phys. Rev. D **103**, 013002 (2021).

[8] A. Costantini, F. De Lillo, F. Maltoni, L. Mantani, O. Mattelaer, R. Ruiz, and X. Zhao, Vector boson fusion at multi-TeV muon colliders, J. High Energy Phys. 09 (2020) 080.

[9] P. Asadi, R. Capdevilla, C. Cesarotti, and S. Homiller, Searching for leptoquarks at future muon colliders, J. High Energy Phys. 10 (2021) 182; S. Qian, C. Li, Q. Li, F. Meng, J. Xiao, T. Yang, M. Lu, and Z. You, Searching for heavy leptoquarks at a muon collider, J. High Energy Phys. 12 (2021) 047.

[10] T. Han, Z. Liu, L. T. Wang, and X. Wang, WIMPs at high energy muon colliders, Phys. Rev. D **103**, 075004 (2021); R. Capdevilla, F. Meloni, R. Simoniello, and J. Zurita, Hunting wino and higgsino dark matter at the muon collider with disappearing tracks, J. High Energy Phys. 06 (2021) 133.

[11] R. Essig *et al.*, Working group report: New light weakly coupled particles, arXiv:1311.0029; J. Alexander *et al.*, Dark sectors 2016 workshop: Community report, arXiv:1608.08632; M. A. Deliyergiyev, Recent progress in search for dark sector signatures, Open Phys. **14**, 281 (2016).

[12] B. Holdom, Two U(1)'s and ϵ charge shifts, Phys. Lett. **166B**, 196 (1986).
[13] M. Fabbrichesi, E. Gabrielli, and G. Lanfranchi, *The Physics of the Dark Photon. A Primer*, Springer Briefs in Physics (Springer Nature, Switzerland, 2020), 10.1007/978-3-030-62519-1.
[14] B. A. Dobrescu, Massless Gauge Bosons Other than the Photon, Phys. Rev. Lett. **94**, 151802 (2005).
[15] E. Gabrielli, B. Mele, M. Raidal, and E. Venturini, FCNC decays of standard model fermions into a dark photon, Phys. Rev. D **94**, 115013 (2016).
[16] R. D. Peccei and H. R. Quinn, *CP* Conservation in the Presence of Instantons, Phys. Rev. Lett. **38**, 1440 (1977).
[17] S. Weinberg, A New Light Boson?, Phys. Rev. Lett. **40**, 223 (1978).
[18] F. Wilczek, Problem of Strong P and T Invariance in the Presence of Instantons, Phys. Rev. Lett. **40**, 279 (1978).
[19] L. Bento, J. C. Romao, and A. Barroso, $e^+e^- \to \gamma +$ missing neutrals: Neutrinos versus photino production, Phys. Rev. D **33**, 1488 (1986).
[20] F. A. Berends, G. J. H. Burgers, C. Mana, M. Martinez, and W. L. van Neerven, Radiative corrections to the process $e^+e^- \to$ neutrino anti-neutrino γ, Nucl. Phys. **B301**, 583 (1988).
[21] N. Chakrabarty, T. Han, Z. Liu, and B. Mukhopadhyaya, Radiative return for heavy Higgs boson at a muon collider, Phys. Rev. D **91**, 015008 (2015).
[22] K. Mimasu and V. Sanz, ALPs at colliders, J. High Energy Phys. 06 (2015) 173.
[23] M. Bauer, M. Heiles, M. Neubert, and A. Thamm, Axion-like particles at future colliders, Eur. Phys. J. C **79**, 74 (2019).
[24] S. Biswas, A. Chatterjee, E. Gabrielli, and B. Mele, Probing dark-axion like particle portals at future e^+e^- colliders, Phys. Rev. D **100**, 115040 (2019).
[25] L. Darmé, F. Giacchino, E. Nardi, and M. Raggi, Invisible decays of axion-like particles: Constraints and prospects, J. High Energy Phys. 06 (**2021**) 009.
[26] G. Abbiendi *et al.* (OPAL Collaboration), Search for anomalous photonic events with missing energy in e^+e^- collisions at $\sqrt{s} = 130$, 136 and 183 GeV, Eur. Phys. J. C **8**, 23 (1999).
[27] P. Achard *et al.* (L3 Collaboration), Single photon and multiphoton events with missing energy in e^+e^- collisions at LEP, Phys. Lett. B **587**, 16 (2004).
[28] J. Abdallah *et al.* (DELPHI Collaboration), Photon events with missing energy in e^+e^- collisions at $s^{**}(1/2) =$ 130 GeV to 209 GeV, Eur. Phys. J. C **38**, 395 (2005).
[29] T. Aaltonen *et al.* (CDF Collaboration), Search for Large Extra Dimensions in Final States Containing One Photon or Jet and Large Missing Transverse Energy Produced in $p\bar{p}$ Collisions at $\sqrt{s} = 1.96$-TeV, Phys. Rev. Lett. **101**, 181602 (2008).
[30] V. M. Abazov *et al.* (D0 Collaboration), Search for Large Extra Dimensions via Single Photon Plus Missing Energy Final States at $\sqrt{s} = 1.96$-TeV, Phys. Rev. Lett. **101**, 011601 (2008).
[31] M. Aaboud *et al.* (ATLAS Collaboration), Search for new phenomena in events with a photon and missing transverse momentum in pp collisions at $\sqrt{s} = 13$ TeV with the ATLAS detector, J. High Energy Phys. 06 (2016) 059.
[32] A. M. Sirunyan *et al.* (CMS Collaboration), Search for new physics in final states with a single photon and missing transverse momentum in proton-proton collisions at $\sqrt{s} = 13$ TeV, J. High Energy Phys. 02 (2019) 074.
[33] A. Ringwald, Axions and axion-like particles, arXiv: 1407.0546.
[34] R. Bollig, W. DeRocco, P. W. Graham, and H. T. Janka, Muons in Supernovae: Implications for the Axion-Muon Coupling, Phys. Rev. Lett. **125**, 051104 (2020); **126**, 189901(E) (2021).
[35] F. D'Eramo, R. Z. Ferreira, A. Notari, and J. L. Bernal, Hot axions and the H_0 tension, J. Cosmol. Astropart. Phys. 11 (2018) 014.
[36] M. Pospelov, Secluded U(1) below the weak scale, Phys. Rev. D **80**, 095002 (2009).
[37] M. Escudero, D. Hooper, G. Krnjaic, and M. Pierre, Cosmology with a very light $L_\mu - L_\tau$ gauge boson, J. High Energy Phys. 03 (2019) 071.
[38] D. Banerjee *et al.* (NA64 Collaboration), Search for Axion-like and Scalar Particles with the NA64 Experiment, Phys. Rev. Lett. **125**, 081801 (2020).
[39] J. Abdallah *et al.* (DELPHI Collaboration), Search for one large extra dimension with the DELPHI detector at LEP, Eur. Phys. J. C **60**, 17 (2009).
[40] J. P. Lees *et al.* (*BABAR* Collaboration), Search for invisible decays of a dark photon produced in e^+e^- collisions at *BABAR*, Phys. Rev. Lett. **119**, 131804 (2017).
[41] E. Kou *et al.* (Belle-II Collaboration), The Belle II physics book, Prog. Theor. Exp. Phys. **2019**, 123C01 (2019); **2020**, 029201 (2020).
[42] M. J. Dolan, T. Ferber, C. Hearty, F. Kahlhoefer, and K. Schmidt-Hoberg, Revised constraints and Belle II sensitivity for visible and invisible axion-like particles, J. High Energy Phys. 12 (2017) 094; 03 (2021) 190(E).
[43] J. D. Bjorken, S. Ecklund, W. R. Nelson, A. Abashian, C. Church, B. Lu, L. W. Mo, T. A. Nunamaker, and P. Rassmann, Search for neutral metastable penetrating particles produced in the SLAC beam dump, Phys. Rev. D **38**, 3375 (1988).
[44] N. Bartosik *et al.*, Preliminary Report on the study of beam-induced background effects at a muon collider, arXiv: 1905.03725v1; F. Collamati *et al.*, Advanced assessment of beam induced background at a muon collider, arXiv: 2105.09116.
[45] N. Bartosik *et al.*, Detector and physics performance at a muon collider, J. Instrum. **15**, P05001 (2020).
[46] N. Bartosik *et al.*, Full detector simulation with unprecedented background occupancy at a muon collider, Comput. Software Big Sci. **5**, 21 (2021).
[47] J. Alwall, R. Frederix, S. Frixione, V. Hirschi, F. Maltoni, O. Mattelaer, H.-S. Shao, T. Stelzer, P. Torrielli, and M. Zaro, The automated computation of tree-level and next-to-leading order differential cross sections, and their matching to parton shower simulations, J. High Energy Phys. 07 (2014) 079.
[48] T. Sjostrand, S. Mrenna, and P. Z. Skands, PYTHIA6.4 physics and manual, J. High Energy Phys. 05 (2006) 026.
[49] T. Sjöstrand, S. Ask, J. R. Christiansen, R. Corke, N. Desai, P. Ilten, S. Mrenna, S. Prestel, C. O. Rasmussen, and P. Z. Skands, An introduction to PYTHIA8.2, Comput. Phys. Commun. **191**, 159 (2015).

[50] M. Frank, F. Gaede, C. Grefe, and P. Mato, DD4hep: A detector description toolkit for high energy physics experiments, J. Phys. Conf. Ser. **513**, 022010 (2014).; F. Gaede *et al.*, LCIO: A persistency framework for linear collider simulation studies, CHEP-2003-TUKT001, arXiv:physics/0306114v1; F. Gaede, Marlin and LCCD–Software tools for the ILC, Nucl. Instrum. Methods Phys. Res., Sect. A **559**, 177 (2006).

[51] Detector Technologies for CLIC, edited by D. Dannheim, K. Krüger, A. Levy, A. Nürnberg, and E. Sicking, Report No. CERN-2019-001, CERN, Geneva, 2019, 10.23731/CYRM-2019-001.

[52] J. S. Marshall and M. A. Thomson, The Pandora software development kit for pattern recognition, Eur. Phys. J. C **75**, 439 (2015).

[53] The muon collider detector design and performance group, https://muoncollider.web.cern.ch/design/muon-collider-detector.

[54] https://automeris.io/WebPlotDigitizer.